

Theoretical Studies on the Physics of Magnetic Islands

Q. Yu

Max-Planck-Institut für Plasmaphysik, EURATOM Association, D-85748 Germany
email: qiy@ipp.mpg.de

Three aspects of the physics of magnetic islands are investigated. (a) *The threshold for the onset of the island in tokamak plasmas.* For a sufficiently high temperature plasma like that of ASDEX-Upgrade, the stability of a small island is found to be mainly determined by the electron diamagnetic drift frequency ω_{*e} and the heat diffusivity, and it can be driven unstable by the electron temperature gradient for a certain range of ω_{*e} . In the nonlinear stage the saturated island width decreases for sufficiently large ω_{*e} . (b) *The heat diffusion across stochastic magnetic field.* With the increase of the ratio between the parallel and the perpendicular heat diffusivity, the enhanced radial heat diffusivity due to the parallel transport along the field lines is found to be determined first by the additive effect of individual islands and then by the field ergodicity. (c) *The stabilization of the island by rf current drive.* When the rf wave deposition width is larger than the island width, the modulated rf current drive has a stronger stabilizing effect than a non-modulated one. A more effective way for stabilizing the large island is found by using both a rf current drive and a resonant helical field.

1. Introduction

The onset of magnetic islands in tokamak plasmas usually has a significant effect on the plasma performance, which could lead to the confinement degradation, a local stochastic magnetic field region (the frequently interrupted regime), mode locking, or even disruptions [1-5]. It is important to have a better understanding of the physics associated with magnetic islands. Three aspects of the island physics are investigated here: the threshold for the onset of magnetic island, the heat diffusion across a local stochastic magnetic field and the stabilization of the island by localized rf current drive.

2. Threshold for the Onset of Magnetic Island

Most neoclassical tearing modes (NTMs) observed on ASDEX-Upgrade and DIII-D are triggered by additional perturbations like sawteeth [2-5]. This phenomenon agrees with previous theories. Tearing modes are predicted to be stabilized by the electron diamagnetic drift in linear stage in a high β plasma even for $\Delta' > 0$ [6]. The experimental values of Δ' are usually found to be negative for the tearing modes with poloidal mode number $m \geq 3$. In the nonlinear stage the diamagnetic drift effect leads to the ion polarization current model of the threshold for the onset of NTMs [7,8]. In some discharges on ASDEX-Upgrade, however, NTMs grow spontaneously [5]. Moreover, most NTMs observed on TFTR do not have additional triggers for their onset [9], indicating that tearing modes can be linear unstable. It was recently found that, the tearing mode stability depends on both the electron heat transport and the electron diamagnetic drift frequency ω_{*e} [10].

Here the numerical modelling of the tearing mode stability is carried out basing on two fluid equations and using the experimental data as the input. The large aspect-ratio tokamak approximation is utilized, with the magnetic field $\mathbf{B} = B_{0t} - (kr/m)B_{0t}\mathbf{e}_\theta + \nabla\psi \times \mathbf{e}_t$, where ψ is the helical flux function, m/r and $k=n/R$ are the wave vectors in \mathbf{e}_θ (poloidal) and \mathbf{e}_t (toroidal) direction, respectively, and the subscript 0 denotes an equilibrium quantity. The ion velocity $\mathbf{v} = u\mathbf{e}_\parallel + \mathbf{v}_\perp$, where u and $\mathbf{v}_\perp = \nabla\phi \times \mathbf{e}_t$ are the parallel and the perpendicular component. To obtain ψ , u , \mathbf{v}_\perp , the electron density n_e and temperature T_e , the following two fluid equations in normalized units are utilized [6,10],

$$\frac{dn_e}{dt} = d_1 \nabla_{\parallel} j - \nabla_{\parallel} (n_e u) + \nabla \cdot (D_{\perp} \nabla_{\perp} n_e) + S_n, \quad (1)$$

$$\frac{d\psi}{dt} = -\eta(j - j_b - j_d) + \Omega[\nabla_{\parallel} n_e + 1.17(1 + \alpha)J\nabla_{\parallel} T_e + E_{\phi}] \quad (2)$$

$$\frac{du}{dt} = -\frac{C_s^2}{n_e} \nabla_{\parallel} (n_e T_e) + \mu_{\perp} \nabla_{\perp}^2 u, \quad (3)$$

$$\frac{d}{dt} \nabla_{\perp}^2 \phi = S^2 \nabla_{\parallel} j + \mu_{\perp} \nabla_{\perp}^4 \phi, \quad (4)$$

$$\frac{3}{2} n_e \frac{dT_e}{dt} = d_1 (1 + \alpha) \nabla_{\parallel} j - T_e n_e \nabla_{\parallel} u + n_e \nabla \cdot (\chi_{\parallel} \nabla_{\parallel} T_e) + n_e \nabla \cdot (\chi_{\perp} \nabla_{\perp} T_e) + S_p, \quad (5)$$

where $d/dt = \partial/\partial t + \mathbf{v}_{\perp} \cdot \nabla$, j , j_b , and j_d are the plasma, the bootstrap and the rf current density along the \mathbf{e}_t direction, respectively. μ_{\perp} is the viscosity, and χ and D are the heat and particle diffusivity. The subscripts \parallel and \perp stand for the parallel and the perpendicular components, and $\alpha = 0.71$ [6,10]. S_n , S_p and E_0 are the particle and heat source and the equilibrium electric field. The parameters in Eqs. (1)-(5) are $d_1 = \omega_{ce}/v_{ei}$, $\Omega = \beta_e d_1$, $\beta_e = 4\pi n_e T_e / B^2$, $C_s = [(T_e + T_i)/m_i]^{1/2} a / \tau_R$, $S = \tau_R / \tau_A$, where $\tau_A = a / v_A$ is the Alfvén time, and $\tau_R = a^2 \mu_0 / \eta(r=0)$ is the resistive time. The length is normalized to the minor radius a , the time t to τ_R , ψ to $a B_{0t}$, \mathbf{v} to a / τ_R , and T_e and n_e to their values at $r=0$. Eqs. (1)-(5) was utilized to study the tearing mode stability before by neglecting the perpendicular transport [6].

An example of the spontaneous growing $m/n=3/2$ tearing mode on ASDEX-Upgrade was shown in Ref. [5]. The corresponding deuterium plasma has $T_e = 3.25 \text{ keV}$, $n_e = 1.15 \times 10^{20} \text{ m}^{-3}$ and $B_{0t} = 2 \text{ T}$, leading to $S = 4.27 \times 10^8$, $d_1 = 2.7 \times 10^7$, $\Omega = 8.45 \times 10^5$, $C_s = 1.01 \times 10^8 a / \tau_R$, and $\chi_{\parallel} = 1.11 \times 10^{13} a^2 / \tau_R$. The local equilibrium density gradient is nearly zero, and $L_{Te} = T_{e0} / [a(dT_{e0}/dr)] = 0.41$ at the $q=3/2$ rational surface. The profile of the safety factor q is monotonic with a negative value of Δ' for the $3/2$ mode. Above parameters provide the input data for our numerical calculations.

In Fig. 1a the normalized linear growth rate γ of the $3/2$ mode is shown as a function of the parameter Ω by the solid curve for $D_{\perp} = \chi_{\perp} = 0.3 a^2 / \tau_R$ and $\mu_{\perp} = 18.3 a^2 / \tau_R$. The classical perpendicular electron heat conductivity, $\chi_{\perp} = 4.7 v_e (v_{Te} / \omega_{ce})^2$, leads to $\chi_{\perp} = 0.3 a^2 / \tau_R$. From Eq. (2) $\omega_{*e} = \Omega [n_{e0}' + 1.17(1 + \alpha) T_{e0}'] m / r_s$ is found, where the prime denotes d/dr , and r_s is the minor radius at the rational surface. A larger Ω value corresponds to a larger ω_{*e} or a higher β value. For a sufficiently small Ω the diamagnetic drift effect is not important, and $\gamma = -2.0 \times 10^3 / \tau_R$ when $\Omega = 0$. For a sufficiently large Ω , corresponding to a high mode frequency, the mode is very stable with large negative values of γ , in agreement with previous theories that the tearing mode is stable for sufficiently large ω_{*e} [6]. For intermediate value of Ω around $10^5 < \Omega < 10^6$, however, the mode becomes unstable, which is different from previous results [6]. The experimental value of $\Omega = 8.45 \times 10^5$ as mentioned above lies in the unstable region, in agreement with the experimental result that the $3/2$ mode grows spontaneously. The dotted curve in Fig. 1a is obtained by taking $D_{\perp} = \chi_{\perp} = 0.1 a^2 / \tau_R$. The unstable region is narrower as χ_{\perp} decreases. The dashed curve in Fig. 1a shows the growth rate of the $6/4$ mode. The $6/4$ mode has nearly the same unstable region as the $3/2$ mode. Only in the small or large Ω region the $6/4$ mode is more stable than the $3/2$ mode.

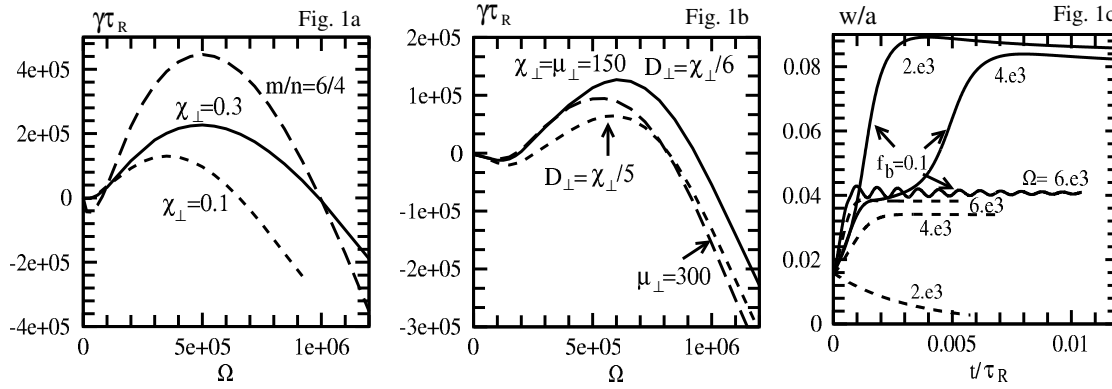


Fig. 1 (a) The normalized linear growth rate versus Ω for classical perpendicular transport coefficients. (b) Same as (a) but for anomalous perpendicular transport coefficients. (c) Nonlinear time evolution of the island width with $f_b=0.1$ (solid) and 0 (dotted) for $\Omega=2, 4$ and 6×10^3 .

Since the perpendicular transport is usually anomalous for tokamak plasmas, we have also studied the mode stability by taking the perpendicular transport coefficients to be at the level of the anomalous transport coefficients. In Fig. 1b the growth rate of the 3/2 mode is shown as a function of Ω by the solid curve for $\chi_{\perp}=\mu_{\perp}=150a^2/\tau_R$ and $D_{\perp}=\chi_{\perp}/6$, corresponding to $\chi_{\perp}=\mu_{\perp}=0.5m^2/s$. It is seen that, the mode remains stable in the small or large Ω region. The dotted curve in Fig. 1b is obtained with $D_{\perp}=\chi_{\perp}/5$, and dashed one with $\mu_{\perp}=300a^2/\tau_R$. A larger D_{\perp} or μ_{\perp} leads to a narrower unstable region. When the equilibrium electron temperature gradient is taken to be zero, no unstable mode is found independent of the values for Ω and the plasma density gradient, indicating that the electron temperature gradient is the only driving mechanism for the unstable mode. Extensive calculations have also been done to study the effect of other parameters. The mode is found to be more unstable for a smaller value of C_s or larger values of d_1 , χ_{\parallel} and S .

The nonlinear time evolution of the normalized island width, W/a , is shown in Fig. 1c with a reduced set of parameters, $S=5\times 10^6$, $d_1=1.0\times 10^5$, $C_s=1.0\times 10^6a/\tau_R$, $\chi_{\parallel}=5.0\times 10^8a^2/\tau_R$, $\chi_{\perp}=\mu_{\perp}=10a^2/\tau_R$, and $D_{\perp}=\chi_{\perp}/5$, for saving the computation time. The other parameters are kept unchanged. It is seen that, when the fraction of the bootstrap current density at the rational surface, $f_b=[j_b/j]_{r=r_s}$, is 0 (dotted curves), the island decays for $\Omega\leq 2\times 10^3$ but grows and saturates for $\Omega=4\times 10^3$ and 6×10^3 . The local electron temperature gradient is decreased by the island, which in turn leads to the mode saturation. For $f_b=0.1$ (solid curves), the mode further develops into the standard NTMs and saturates at a larger amplitude for $\Omega=2\times 10^3$ and 4×10^3 . For a sufficiently large Ω ($\geq 6\times 10^3$), the island width becomes comparable to that obtained with $f_b=0$. When Ω is high enough ($\Omega>2\times 10^4$), the island is found to decay even for $f_b=0.1$, indicating that the ion polarization current could be important in determining the saturation amplitude of NTMs. The mode frequency is found to be proportional to Ω for a small island and decreases as the island width increases due to the partial flattening of the temperature profile across the island.

3. Heat Diffusion across a Local Stochastic Magnetic Field

The heat diffusion across the stochastic field is of general interest in plasma physics [e.g., 3]. It was shown in Ref. [11] that, in the collisional regime $L_{\lambda}<L_{\kappa}$, the enhanced radial heat conductivity due to the magnetic field ergodicity, χ_r , is

$$\chi_r = D_M \chi_{||} / L_{c\delta}, \quad (6)$$

where $D_M = L_0 \sum (b_{r,k} / B_{0r})^2 \delta(m_k/q - n_k)$, $b_{r,k}$, m_k and n_k are the radial field perturbation, the poloidal and toroidal mode numbers of the k th Fourier component, respectively, $L_0 \approx \pi R$, $L_{c\delta} = L_c \ln[(r/mL_c)(\chi_{||}/\chi_{\perp})^{1/2}]$, $L_c = \pi R / \ln(\pi \Delta / 2)$, $\Delta = (w_1 + w_2) / (2|r_1 - r_2|)$, w_1 and w_2 are the widths of two neighboring islands, and r_1 and r_2 are the minor radius of the corresponding rational surfaces. L_{λ} is the electron mean free path, $L_k \approx [L_s^2 / (k_{\perp}^2 D_M)]^{1/3}$ [11,12], k_{\perp} is the perpendicular wave vector of the perturbations, $L_s = Rq^2 / rq'$, and the summation is over k to include all resonant components. Krommes *et al* later showed that the collisional regime consists of three sub-regimes [12]. With the decrease of L_{λ} they are (a) Rechester-Rosenbluth regime, $\chi_r = D_M \chi_{||} / L_k$, (b) Kadomsev-Pogutse regime, $\chi_r = D_M k_{\perp} (\chi_{||} \chi_{\perp})^{1/2}$, and (c) Fluid regime, $\chi_r = D_M \chi_{||} / L_0$. It was found recently that [13], in the limit $\chi_{||} / \chi_{\perp} \gg 1$ but $W_k / W_{c,k} \ll 1$,

$$\chi_r(r) = \sum_k \chi_{\perp} \frac{W_k^4}{8W_{c,k}^4} g_k(z_k) = \sum_k \chi_{||} \frac{b_{r,k}^2}{2B_{0r}^2} g_k(z_k), \quad (7)$$

where W_k is the island width of the k th component, $W_{c,k} = a(\chi_{\perp} / \chi_{||})^{1/4} [8L_q / (\epsilon a n_k)]^{1/2}$, $\epsilon = a/R$, $L_q = q/q'$, $z_k = 2^{3/2}(r - r_{s,k}) / W_{c,k}$, $r_{s,k}$ is the minor radius of the rational surface, $g(z) = [1 + zf(z)]$, and $f(z) = -0.5z \int_0^1 dy (1 - y^2)^{-1/4} \exp(-zy^2/2)$ with integration from 0 to 1. Eq. (7) reduces to the Fluid regime result in the limit $z_k = 0$ except for a factor $2\delta(m_k/q - n_k)$. The function $g_k(z_k)$ in Eq. (7), however, indicates the role of $W_{c,k}$. Since $g_k(z_k)$ approaches zero as $z_k > 2$ [13], χ_r is dominated by the additive effects of these individual islands satisfying $z_k < 2$. This is different from previous theories that D_M includes all resonant perturbations. Eq. (7) has an important implication on the heat diffusion across a stochastic field where $\chi_{||} / \chi_{\perp}$ is not high enough. For typical tokamak edge parameters $T_e = 40 \text{ eV}$, $n_e = 10^{19} \text{ m}^{-3}$, $L_q = a$, $R/a = 3$, $n = 2$ and $\chi_{\perp} = 1 \text{ m}^2/\text{s}$, one finds $W_{c,k} = 0.060a$. This means that for small islands with $W_k < 0.060a$, the heat diffusion is determined by the additive effect of individual islands rather than the field ergodicity.

Numerical simulations can check the analytical result for $W_k / W_{c,k} < 1$ and provide further insight into the χ_r for $W_k > W_{c,k}$. Recently a new numerical method was developed for such a purpose, showing the required numerical accuracy at high $\chi_{||} / \chi_{\perp}$ [14]. Eq. (5) is solved with $u = d_1 = 0$, $q(r) = q_0 \exp(r/L_q)$, $\psi_k(r) = \psi_0 (r/a)^2 (1 - r/a)^2 a B_{0r} \cos(m_k \theta + n_k \phi)$, and the perturbed field $\mathbf{B}_1 = \sum \nabla \psi_k \times \mathbf{e}_t$, assuming n_e , $\chi_{||}$ and χ_{\perp} to be constant. $S_p(r) = P_0 [1 - (r/a)^2]^{16}$ peaks at $r = 0$.

The local magnetic field becomes stochastic when islands of different helicity overlap. In Fig. 2a $\log(\chi_r / \chi_{\perp})$ versus $\log(\chi_{||} / \chi_{\perp})$ is shown for $L_q = 0.3a$ and $\psi_0 = 9 \times 10^{-4}$ by the solid curve for a two island case, $m/n = 3/2$ and $4/3$, leading to the island width $W_{3/2} = W_{4/3} = 0.045a$. The rational surfaces are at $r_{3/2} = 0.604a$ and $r_{4/3} = 0.569a$, with $\Delta = 1.3$. The value of χ_r is taken at $r = 0.587a$ where the field is stochastic. χ_{\perp} is kept constant for these calculations. It is seen that $\chi_r \propto \chi_{||}$ for $\chi_{||} / \chi_{\perp} < 10^6$ in agreement with Eq. (7). For $\chi_{||} / \chi_{\perp} > 3 \times 10^8$ ($W_{3/2} > 3.2W_{c,3/2}$), χ_r also approximately scales as $\chi_{||}$. Between these two limits there is a transition region around $\chi_{||} / \chi_{\perp} = 3 \times 10^7$ ($W_{3/2} = 1.7W_{c,3/2}$) where χ_r slowly increases with $\chi_{||}$. The dotted curve shows $\log(\chi_{3/2} + \chi_{4/3})$, where $\chi_{3/2}$ ($\chi_{4/3}$) is the $(\chi_r / \chi_{\perp})|_{r=0.587a}$ obtained for a single $3/2$ ($4/3$) island alone, with other parameters unchanged. The dotted curve is the same as the solid one for $\chi_{||} / \chi_{\perp} < 3 \times 10^7$, as predicted by Eq. (7) that χ_r is determined by the additive effects of the individual islands for $W_k < W_{c,k}$. Only for $W_k \gg W_{c,k}$, the solid curve is larger than the

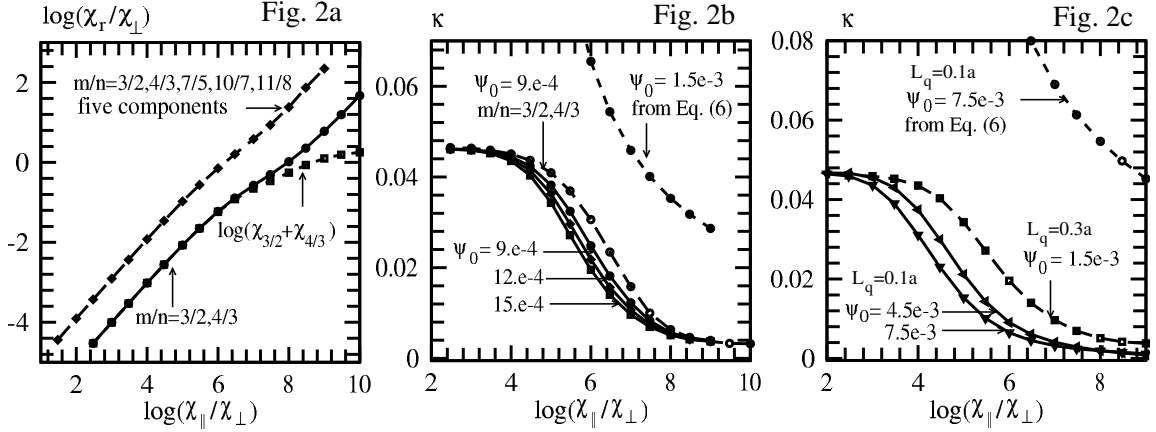


Fig. 2 (a) $\log(\chi_r/\chi_\perp)$ versus $\log(\chi_\parallel/\chi_\perp)$ for two island case, $m/n=3/2$ and $4/3$ (solid). The dotted curve shows $\log(\chi_{3/2} + \chi_{4/3})$, and the dashed curve is the $\log(\chi_r/\chi_\perp)$ for $m/n=3/2, 4/3, 7/5, 10/7,$ and $11/8$. (b) κ versus $\log(\chi_\parallel/\chi_\perp)$ with $\psi_0=0.9, 1.2$ and 1.5×10^{-3} for the 5 islands case (solid). The dotted curve shows the result from Eq. (6) with $\psi_0=1.5 \times 10^{-3}$, and the dashed curve is the κ for $m/n=3/2$ and $4/3$ with $\psi_0=9.0 \times 10^{-4}$. (c) κ versus $\log(\chi_\parallel/\chi_\perp)$ with $L_q=0.1a$ and $\psi_0=4.5$ and 7.5×10^{-3} for the 5 islands case (solid). The dotted curve shows the result from Eq. (6) with $\psi_0=7.5 \times 10^{-3}$, and the dashed curve is the κ for $L_q=0.3a$ and $\psi_0=1.5 \times 10^{-3}$.

dotted one, showing the role of the field ergodicity. The dashed curve in Fig. 2a is the $\log(\chi_r/\chi_\perp)$ at $r=0.579a$ for the same ψ_0 but five components magnetic perturbations, $m/n=3/2, 4/3, 7/5, 10/7,$ and $11/8$, with Δ ranging from 1.6 to 3.8 and $r_{7/4}=0.584a, r_{10/7}=0.590a$ and $r_{11/8}=0.578a$. It shows a similar behavior as the two islands cases.

Since χ_r is not constant across the stochastic field region, in the following the radial averaged χ_r , $\langle \chi_r \rangle = \int \chi_r dr / (r_b - r_a)$, is used for a further comparison with analytical results. The integration is taken from $r_a=0.575a$ to $r_b=0.600a$ where the magnetic field is stochastic. In Fig. 2b $\kappa \equiv a \langle \chi_r \rangle / [\chi_\parallel L_0 \sum (b_{k,r} / B_{0r})^2]$ versus $\log(\chi_\parallel/\chi_\perp)$ is shown by the solid curves with $\psi_0=9 \times 10^{-4}, 1.2 \times 10^{-3},$ and 1.5×10^{-3} for the 5 islands case. For $\chi_\parallel/\chi_\perp \sim 10^2 - 10^3$, κ is the same for different ψ_0 , as predicted by Eq. (7) in the limit $z_k=0$. In this limit Eq. (7) leads to $\kappa=0.048$ in agreement with the numerical results. With the increase of $\chi_\parallel/\chi_\perp$, κ decreases and approaches a steady value again at high $\chi_\parallel/\chi_\perp$ for sufficiently large ψ_0 (κ oscillates for small ψ_0). This differs from the prediction of the Rechester-Rosenbluth regime that $\kappa \sim 1/L_k \sim D_M^{1/3} \sim \psi_0^{2/3}$. The faster decay of κ with increasing $\chi_\parallel/\chi_\perp$ for a larger ψ_0 is due to the corresponding larger $W_k/W_{c,k}$ so that the transition region as shown in Fig. 2a is reached at a lower $\chi_\parallel/\chi_\perp$. The dotted curve on Fig. 2b shows the result from Eq. (6) with $\psi_0=1.5 \times 10^{-3}$, being different from the numerical results. The dashed curve is the κ for the two island case, $m/n=3/2$ and $4/3$, with $\psi_0=9.0 \times 10^{-4}$ and the radial average from $r=0.58a$ to $0.59a$, which shows a similar behavior as the five islands case: κ decreases by about one order of magnitude from small to large $W_k/W_{c,k}$.

Increasing the magnetic shear by 3 times to $L_q=0.1a$, κ versus $\log(\chi_\parallel/\chi_\perp)$ is shown in Fig. 2c by the solid curves for the 5 islands case with $\psi_0=4.5 \times 10^{-3}$ and 7.5×10^{-3} . In this case the rational surfaces are closer, with $r_{3/2}=0.595a, r_{4/3}=0.583a, r_{7/4}=0.588a, r_{10/7}=0.590a$ and $r_{11/8}=0.587a$, and the radial average is from $0.584a$ to $0.594a$. It is seen that κ approaches a

steady value for $\chi_{\parallel}/\chi_{\perp} \sim 10^2$ and a nearly steady value at large $\chi_{\parallel}/\chi_{\perp}$ for sufficiently large ψ_0 , similar to Fig. 2b. The dotted curve is the result from Eq. (6) for $\psi_0 = 7.5 \times 10^{-3}$, being more different from the numerical results for the large magnetic shear case. The dashed curve is the result with a smaller magnetic shear, $L_q = 0.3a$, and $\psi_0 = 1.5 \times 10^{-3}$. It is seen that, with a larger magnetic shear κ converges to a smaller value at large $\chi_{\parallel}/\chi_{\perp}$ for sufficiently large ψ_0 , differing to the prediction of the Rechester-Rosenbluth regime that $\kappa \sim 1/L_k \sim L_q^{-2/3}$. The Kadomsev-Pogutse regime is not found from numerical results.

4. Stabilization of Magnetic Islands by RF Current Drive

To study the stabilization of NTMs by localized rf current drive, the basic equations utilized here are Eqs. (2), (4) and (5), and the two fluids effects are neglected by taking $\Omega = d_1 = C_s = 0$. The fast electron density is described by [15]

$$\frac{\partial n_f}{\partial t} = \nabla \cdot (\chi_{\parallel f} \nabla_{\parallel} n_f) + \nabla \cdot (\chi_{\perp f} \nabla_{\perp} n_f) + v(n_{fs} - n_f), \quad (8)$$

where n_f , $\chi_{\parallel f}$, $\chi_{\perp f}$, and v^{-1} are the density, the parallel and perpendicular transport coefficients, and the slowing down time of the fast electrons, respectively. n_{fs} is the fast electron source due to the rf waves given by [15]

$$n_{fs} = n_{fs0} \exp\left[-\left(\frac{r-r_{ds}}{w_{ds}}\right)^2\right] \Pi(h_0, \Delta h), \quad (9)$$

where n_{fs0} , w_{ds} and r_{ds} specify the magnitude, the radial half-width and the deposition radius of the source, respectively. $\Pi(h_0, \Delta h) = 1$ for $|h - h_0| < \Delta h$ and $h_{on} < h_0 < h_{off}$, and $\Pi(h_0, \Delta h) = 0$ elsewhere, where $h_0 = \omega t$, ω is the rf wave modulation frequency, Δh is the instantaneous wave deposition width along the helical angle $h = m\theta + n\phi$, and h_{on} (h_{off}) is the helical angle at which the rf wave is turned on (off). The frame studied is the one in which the island does not rotate, and its o-point and x-point are at $h = 0^\circ$ and $\pm 180^\circ$ respectively, while the instantaneous wave deposition rotates with respect to the island at an angular frequency ω . When $h_{on} = -90^\circ$ and $h_{off} = 90^\circ$, the wave deposition is only around the island's o-point, and we will call this case as the modulated current drive (MCD). When $h_{on} = -180^\circ$ and $h_{off} = 180^\circ$, the fast electron source rotates all along the helical angle, corresponding to a continuous rf current drive in time. Assuming that the driven current density is proportional to the fast electron density, $j_d \sim n_f$, the total driven current I_d is obtained by integrating j_d over the plasma cross section. The rf source current I_{ds} is obtained similarly.

In Fig. 3a the saturated island width of a $m/n = 3/2$ NTM driven by the bootstrap current is shown by the dotted line, with $r_s = 0.58a$, $f_b = 6.4\%$, $S = 10^8$, $\tau_{\mu} = a^2/\mu_{\perp} = \tau_R/10$, and $\chi_{\parallel}/\chi_{\perp} = 10^{10}$. When the rf current is switched on, the saturated island width is shown as a function of $\alpha = |h_{on} + h_{off}|/2$ for $v = 3 \times 10^3/\tau_R$, $10^4/\tau_R$, $3 \times 10^4/\tau_R$, and $5 \times 10^4/\tau_R$, respectively, with $\alpha_w = |h_{on} - h_{off}|/2 = 90^\circ$ (MCD), $I_{ds}/I_p = 0.03$, $w_{ds}/a = 0.1$, $\chi_{\perp f} = 1.0a^2/\tau_R$, $\chi_{\parallel f}/\chi_{\perp f} = 10^{10}$, $\Delta h = 27.6^\circ$, and $\omega = 3 \times 10^4/\tau_R$. It is seen that a rf current drive around the island's o-point at $\alpha = 0^\circ$ (x-point at $\alpha = 180^\circ$) has a stabilizing (destabilizing) effect. The transition from the stabilization to destabilization occurs around $\alpha = 90-100^\circ$. For a larger v , the stabilizing effect is larger because (a) a larger v/ω leads to a higher I_d/I_{ds} , and (b) A larger v (smaller $\chi_{\perp f}/v$) leads to a weaker broadening of the rf current density profile.

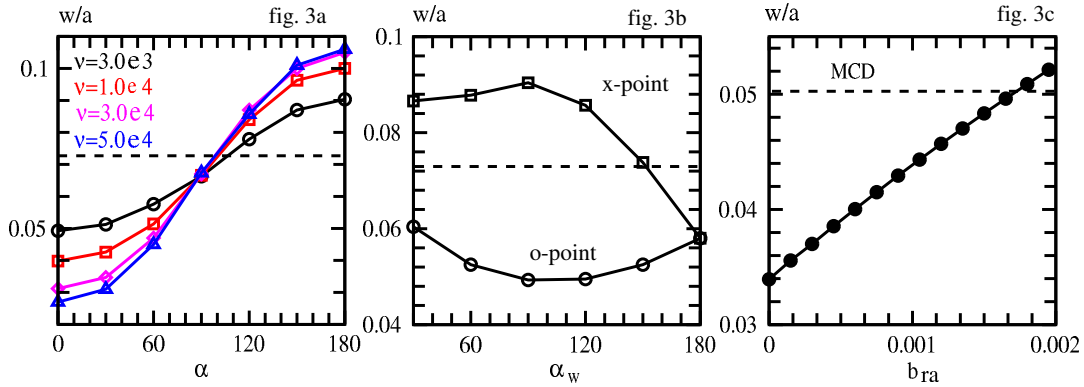


Fig. 3 (a) The saturated island width versus $\alpha = |h_{on} + h_{off}|/2$ without (dotted) and with rf current for $\nu = 0.3, 1, 3$ and $5 \times 10^4 / \tau_R$ (solid). (b) The saturated island width versus $\alpha_w = |h_{on} - h_{off}|/2$ without (dotted) and with rf current for $\alpha = 0^\circ$ (o-point) and 180° (x-point). (c) The saturated island width versus b_{ra} (solid) and the saturated island width obtained for MCD and $b_{ra} = 0$ (dotted).

In Fig. 3b the saturated island width of a $m/n=3/2$ NTM driven by the bootstrap current is shown by the dotted line. When the rf current is switched on, the saturated island width is shown as a function of $\alpha_w = |h_{on} - h_{off}|/2$ for $\alpha = 0^\circ$ (o-point) and 180° (x-point), with other parameters unchanged. It is seen that for $\alpha = 0^\circ$, the largest stabilizing effect is around $\alpha_w = 90^\circ$ (MCD). For $\alpha_w = 180^\circ$ (continuous current drive), the stabilizing effect is weaker than the MCD to deposit the rf current around the island's o-point, since the rf deposition width is larger than the island width [15].

It is well known that it is more favorable for a fusion reactor to operate at a higher β value. In the high β regime the $m/n=2/1$ NTM is expected to develop into a larger amplitude [2]. Comparing with the $3/2$ mode, the $2/1$ mode is closer to the plasma edge and can be easily locked to the wall or the error field when the island is large enough. Once mode locking occurs, its stabilization by rf current is usually not possible, since the o-point of a locked island is not necessarily in the deposition region of the rf wave. To use the rf current to stabilize a locked mode, an externally applied resonant helical field (RHF) is needed to adjust the island to be in the right phase. There are extensive studies on the mode locking of tearing modes. The experimental results show that the penetration threshold of an error field is very small, typically $b_{ra} = b_r(r=a)/B_{0r} < 10^{-4}$ [16,17]. For the mode locking of a large island to a RHF, the required amplitude of RHF is much smaller, since the electromagnetic torque to stop the island rotation increases with the square of the island width. Here the mode locking will not be studied, and we only focus on the effect of the RHF on the stabilization of the locked NTMs by the rf current.

In Fig. 3c the saturated island width of the $3/2$ mode is shown as a function of b_{ra} for $f_b = 0.19$, $I_{ds} = 0.06$, and $w_{ds} = 0.05a$ (solid curve). In this case mode locking is assumed for all values of b_{ra} by taking $\omega = 0$, so that the island's o-point is always in the center of the rf wave deposition region. The island width increases with b_{ra} , since the RHF has a destabilizing effect on NTMs after mode locking. The dotted line shows saturated island width obtained for MCD with $b_{ra} = 0$, $\omega = 3 \times 10^4 / \tau_R$ and other parameters unchanged. In the MCD case, the rf power is turned on for only half the time (see Fig. 3b), and the resulting rf current is only half of that of a continuous current drive. With a RHF the island width is reduced to a smaller value by the rf current than that of MCD for $b_{ra} < 1.8 \times 10^{-3}$, because after mode locking the rf power is turned on for the full time, and the rf current is two times

larger than that of MCD, leading to a larger stabilizing effect comparing with MCD if the required b_{ra} to lock island is not too large.

In fact, when the amplitude of the RHF is large enough to decrease the island rotation frequency, leading to a longer island rotation period comparing with the slowing down time of the fast electrons, a larger stabilizing effect by the rf current is expected as seen from Fig. 3a. Above results indicate that, the RHF can not only be used to adjust the island phase to let its o-point in the rf wave deposition region after usual mode locking, it can also be actively used to increase the stabilizing efficiency of the rf current, once the island is large enough so that a small amplitude RHF can decrease the island rotation frequency or lock the island in the desired phase. Such a method is expected to be helpful for the stabilization of NTMs, especially the 2/1 NTM, in the plasma with a higher bootstrap current fraction.

5. Summary

(a) Using the experimental values as the input data, the electron temperature gradient is shown to drive a new type of tearing mode instability even for a negative Δ' , in agreement with the experimental observations. In the nonlinear phase the saturated island width decreases for sufficiently large electron diamagnetic drift frequency.

(b) The heat diffusion across a local stochastic magnetic field is characterized by $W_k/W_{c,k}$. For the quasi-linear regime $W_k \ll W_{c,k}$, the heat transport is determined by the additive effects of the individual islands. Around $W_k \sim W_{c,k}$, χ_r slowly increases with $\chi_{||}/\chi_{\perp}$. For $W_k/W_{c,k} \gg 1$, χ_r approximately scales with $\chi_{||}$.

(c) When the rf wave deposition width is larger than the island width, the modulated rf current drive has a stronger stabilizing effect than a non-modulated one. The stabilization of a large island by the rf current becomes more effective when using a small amplitude resonant helical field to decrease the island rotation frequency or to lock the island in the rf wave deposition region.

Acknowledgment: I am grateful to Prof. S. Günter and K. Lackner for helpful discussions.

- [1] J. A. Wesson *et al.*, Nucl. Fusion **29** (1989) 641.
- [2] H. Zohm, G. Gantenbein, A. Gude, S. Günter *et al.*, Phys. Plasmas **8** (2001) 2009.
- [3] S. Günter *et al.*, Phys. Rev. Letters **87**, (2001) 275001.
- [4] R. J. La Haye, L. L. Lao, E.J. Strait, and T. S. Taylor, Nucl. Fusion **37** (1997) 397.
- [5] A. Gude, S. Günter, S. Sesnic, ASDEX Upgrade Team, Nucl. Fusion **39** (1999) 127.
- [6] J.F. Drake, *et al.*, Phys. Fluids **26** (1983) 2509.
- [7] A.I. Smolyakov, Plasma Phys. Control. Fusion **35** (1993) 657.
- [8] H.R. Wilson, J.W. Connor, R.J. Hastie, and C.C. Hegna, Phys. Plasmas **3** (1996) 248.
- [9] E.D. Fredrickson, Phys. Plasmas **9** (2002) 548.
- [10] Q. Yu, S. Günter, B.D. Scott, Phys. Plasmas **10** (2003) 797.
- [11] A.B. Rechester and M.N. Rosenbluth, Phys. Rev. Letters **40** (1978) 38.
- [12] J.A. Krommers, C. Oberman and R.G. Kleva, J. Plasma Physics **30** (1983) 11.
- [13] Q. Yu, Phys. Plasmas **13** (2006) 062310.
- [14] S. Günter, Q. Yu, J. Krüger and K. Lackner, J. Comp. Phys. **209** (2005) 35.
- [15] Q. Yu, X.D. Zhang and S. Günter, Phys. Plasmas **11** (2004) 1960.
- [16] R.J. Buttery, *et al.*, Nucl. Fusion **40** (2000) 807.
- [17] R.J. La Haye, A.W. Hyatt, J.T. Scoville, Nucl. Fusion **32** (1992) 2119.